A Rapid and Accurate Switch from RANS to LES in Boundary Layers Using an Overlap Region

Article *in* Flow Turbulence and Combustion · March 2011

DOI: 10.1007/s10494-010-9309-9

CITATIONS
22

READS
258

4 authors:

Michael L. Shur
Peter the Great St.Petersburg Polytechnic University
111 PUBLICATIONS **4,545** CITATIONS
SEE PROFILE

Philippe Spalart
The Boeing Company
230 PUBLICATIONS **19,661** CITATIONS
SEE PROFILE

Michael Strelets
Peter the Great St. Petersburg Polytechnical University, St. Petersburg, Russia
183 PUBLICATIONS **6,384** CITATIONS
SEE PROFILE

A. Travin
Peter the Great St.Petersburg Polytechnic University
57 PUBLICATIONS **3,623** CITATIONS
SEE PROFILE

Flow Turbulence Combust (2011) 86:179–206
DOI 10.1007/s10494-010-9309-9

A Rapid and Accurate Switch from RANS to LES in Boundary Layers Using an Overlap Region

Michael Shur · Philippe R. Spalart · Michael Strelets · Andrey Travin

Received: 3 February 2010 / Accepted: 2 October 2010 / Published online: 21 October 2010

Abstract An efficient recycling algorithm is developed for injecting resolved turbulent content in a boundary layer as it switches from a Reynolds Averaged Navier-Stokes (RANS) type treatment to a Large Eddy Simulation (LES) type treatment inside a generalized Detached-Eddy Simulation (DES). The motivation is to use RANS in the thinnest boundary-layer area, following the original argument in favour of DES, and LES in the thicker boundary-layer areas especially approaching separation, to improve accuracy and possibly obtain unsteady outputs. The algorithm relies on an overlap of the RANS and LES domains and, therefore, the availability of both RANS and LES solutions in the recycling region, which is about 5 boundary-layer thicknesses long. This permits a smooth transfer of the turbulent stresses from this section to the LES inflow. The continuity of the skin-friction distribution is very good, reflecting the excellent viability of the resolved turbulence. The approach is validated in a flat-plate boundary layer and an airfoil near stall, with mild pressure gradient near the interface, and then applied to the compressible flow over an idealized airliner windshield wiper. The pressure fluctuations at reattachment are 12dB more intense than under a simple boundary layer at the same speed, and the output contains all the quantities needed to calculate the transmission of sound through the glass.

Keywords RANS-LES coupling · IDDES · Inflow turbulent content · Recycling

M. Shur · M. Strelets (✉) · A. Travin
New Technologies and Services, 197198, St.-Petersburg, Russia
e-mail: strelets@mail.rcom.ru

P. R. Spalart
Boeing Commercial Airplanes, Seattle, WA, USA

1 Introduction

It is now well established that in flows with any complexity and especially with massive separation, carefully conducted and well-resolved LES is capable of yielding predictions substantially superior to those of RANS models. Thus LES is the preferred route, especially when details of the turbulent structures are needed (aero-acoustics, fluid-structure interaction, etc.), as opposed to only average pressures, for instance. However the cost of such high-quality LES, resolving turbulent structures down to the wall in all turbulent regions is unbearable for high-Reynolds number applications in Aerospace and elsewhere, which have large areas with thin boundary layers [1]. This serious resource problem is increasingly addressed by a variety of hybrid RANS-LES methodologies, driven by the following expectation: the substantial efficiency to be gained if one can use RANS in a large part of the computational domain, where it is trustworthy, and only resort to LES in the sub-domain where accuracy in the face of complexities such as separation, curvature, or vortices, or information on turbulent structures is essential. Once this goal is achieved, together with the continuous increase of computer power, this could enable a substantial re-orientation of applied turbulence-modelling practice, relative to what we have seen for the past 25 years.

Although the spectrum of approaches that are being developed is wide, reflecting the immature stage of the research, two major directions of effort towards generalizing these hybrid methods can be distinguished.

The first one is associated with methods that couple RANS in the very near wall flow region with LES in the outer part of the turbulent layer (and of course the separated regions). These "LES above RANS" methods include versions of Detached-Eddy Simulation (DES) [1], an approach initially meant to treat the whole attached boundary layer by RANS and activate LES only in separated flow regions but then extended [2], and different Wall-Modelled LES (WMLES) approaches [3–6], which treat with RANS only a very shallow part of the whole boundary layer. In a sense, the use of RANS-inspired models very near the wall is a return to the early days of wall-bounded LES in the 1970's, since wall functions were often used. Wall-resolved (as opposed to wall-modelled) LES dominated in the interim, but its reach in Reynolds number is not much larger than that of DNS [1], and the expectations in terms of Reynolds number for most applications make Wall Modelling unavoidable.

An example of the second direction, called embedded LES, involves inserting local LES areas into a global RANS simulation [6], for instance, limiting the LES area only to the trailing-edge region of an airfoil while treating all the rest of the flow with RANS. This may be dubbed "LES after RANS," although some studies also envision "RANS after LES" which will be natural after reattachment. Examples include the flow along the side of a bus, or the surface of an aircraft downstream of an open cavity. Unfortunately, in contrast with the wall-modelling situation [7], the convenient non-zonal pure DES approach does not spontaneously achieve "LES after RANS" behaviour, even if the user gives the equations strong "signals" via the grid density. This also applies to other non-zonal hybrids (e.g., [8, 9]). Note that zonal approaches are much more troublesome for the user, and that their practical application in complex industrial flows is a far from trivial and sometimes insoluble task. On the other hand, in case of success the accuracy gain can be huge and justify the effort.

In this work we are engaged exactly in this second major field, namely "LES downstream of RANS" methods. We stress that the two regions are tightly coupled to calculate the flow around a non-trivial shape, say a wing or a car. This requirement contrasts with the easier problems that arise in very simple geometries: for instance, turbulent channel flow can be generated by a precursor simulation with periodic conditions, and then fed to a simulation of a diffuser with plane-channel inflow. The specific difficulty is finding a simple and robust way to trigger turbulent content at the RANS-to-LES interface. DES is capable of this if the separation is abrupt, for instance with a splitter plate or backward-facing step (even then, the quality of the initial free-shear turbulence is debatable). In an attached boundary layer, in contrast, starting LES with no intentionally added turbulent content would inevitably result in a poor solution. Simply connecting a statistically averaged (RANS) solution with the potential instantaneous LES field along an arbitrary interface, even if the eddy viscosity drops radically, driven by a drop in the grid spacing, cannot be expected to allow fluctuations to emerge naturally and rapidly enough (actually this issue is closely related to the more general problem of providing turbulent inflow conditions for any LES or DNS, unless the incoming flow is laminar). The turbulence would be very weak over many boundary-layer thicknesses. Therefore, when the flow leaves a RANS or Unsteady RANS (URANS) region and enters an LES region, turbulent fluctuations at full strength and of the best possible quality must be superimposed on the RANS values so as not to interrupt the activity and development of the boundary layer. Resolved turbulence must effectively replace the modelled turbulence. Currently, a number of approaches to do this are available, which can be divided into two large groups.

The first group relies upon the use of external databases from LES or DNS of the channel or other, more complex, flows; or else on different types of "synthetic turbulence" (e.g., [9–11]) or on creating approximate turbulence with the use of a vortex method in the transverse plane, which injects some dynamics into the system [12]. External databases are undesirable in practice, due to the great value of having a self-sufficient method capable of high Reynolds numbers, based on the thickness of the shear flow and, even more, the lateral extent on the simulation which is often much larger than that thickness. Synthetic methods, even after recent improvements [11], often fail to produce the near-immediate self-sustaining turbulence that is needed.

An alternative approach to creating turbulent content at the RANS-to-LES interface involves allowing the RANS and LES fields to overlap over some distance. In this case the two fields coexist on the same grid, so that natural turbulent content available in the interior of the LES field can be somehow "transferred" upstream to the interface, only slightly altered. This is inspired by the efficient approach of Lund et al. [13] for providing the inflow boundary conditions in the pure DNS or LES of a simple boundary layer (a simplified version of their approach was also successfully applied in [14] for DNS of complex flows with large-eddy-break-up devices). A major advantage of the recycling idea is that unlike the approaches of the first group, it does not require any outside information and has fewer constraints associated with specific flow peculiarities. On the other hand, it is not naturally self-starting. Considering this, in the present work an attempt is made to develop an accurate and efficient recycling algorithm for the rapid development of high-quality turbulent content at the RANS-LES interface in embedded LES of complex flows. High-quality LES content is

recognized by the production of correct Reynolds stresses at the interface and, which is more challenging, by sustaining them into the LES region. This requires the correct length and time scales and phase relationships in all directions; in other words, "the correct eddies." It is known that random numbers, for instance, fail grossly at this. An easy way to exhibit the failure to achieve this is to detect a sagging skin friction, due to non-viable pseudo-turbulence decaying while viable turbulence is being produced. While the local skin friction may not be of great importance in itself, the issue is the damage done to the boundary-layer thickness, which has strong leverage when entering an adverse pressure gradient.

In Section 2 we present a detailed description of the newly developed recycling procedure, in the framework of boundary layers with mild pressure gradients (which earlier recycling methods did not accommodate), but homogeneous in the lateral direction. Then in Section 3 results are presented of the approach validation and in Section 4 it is applied to an industrial problem, the embedded LES of the flow over a simplified airliner windshield wiper.

2 Description of the Recycling Procedure

2.1 General formulation

Consider a turbulent boundary layer in the coordinate system x (streamwise coordinate), y (wall-normal coordinate) and z (spanwise coordinate). Let both RANS and LES solutions be simultaneously defined in some streamwise region of the boundary layer which includes the sections $x = x_1$ ("Section 1", RANS-LES interface or LES inflow section) and $x = x_2$ ("Section 2" or "recycling section" located in the LES region upstream of the end of the RANS region). These notations are illustrated in Fig. 1, where the overlapping RANS and LES zones are shown from the simulation of a zero-pressure-gradient boundary layer (ZPG BL) performed with the use of the new recycling procedure.[1]

The objective is to "transfer" turbulent fluctuations from the recycling section (Section 2) to the LES inflow section (Section 1) in a manner that allows a seamless transition from a RANS solution to an LES one. The RANS field may not be exactly steady, but at the most it responds to a large-scale temporal dependence of the flow, for instance due to vortex shedding or unsteady boundary conditions. Since the RANS and LES fields overlap over some distance and coexist on the same grid, the streamwise velocity component at some spanwise position z can be "recycled" from the Section 2 to 1 in the following manner (other velocity components are transferred similarly, and the z and t dependence is implied)

$$\left[u_{LES}(y)\right]_1 = \left[u_{RANS}(y)\right]_1 + \left[u'(y)\right]_1, \tag{1}$$

[1]Note that RANS solution may be obtained either independently (in a precursor computation) or in a coupled manner, provided that a code used allows overset grids, which is the case in the present study.

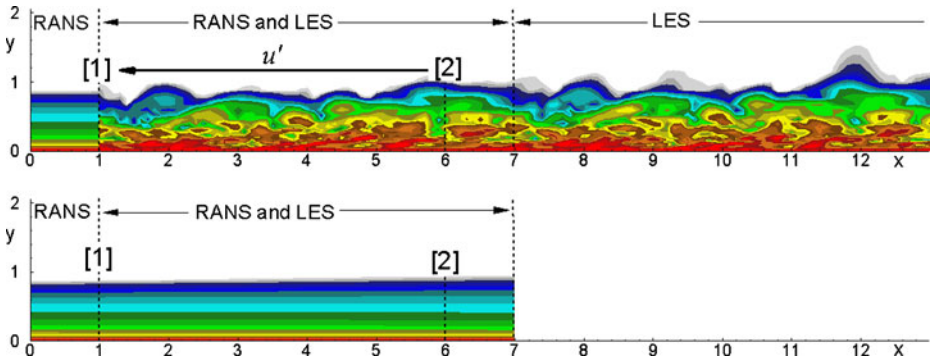

Fig. 1 Schematic of overlapping RANS and LES domains in ZPG BL (coordinates are normalized with the BL thickness at the LES inflow section, δ_0)

where the unknown profile of the velocity fluctuations in the inflow LES section, $\left[u'(y)\right]_1$, is defined using the corresponding fluctuations in the recycling section, $\left[u'(y)\right]_2$, as

$$\left[u'(y)\right]_1 = \alpha \left[u'(y/\beta(y))\right]_2 . \tag{2}$$

Here $\beta(y)$ is a transformation function of the wall-normal coordinate, and α is a scaling coefficient, and both have yet to be defined.

It should be emphasized that the proposed procedure (2) includes recycling of only the fluctuating velocity since the mean velocity field is available in the whole RANS-LES overlapping region. This alone makes it applicable to a much wider spectrum of flows than, e.g., that of Lund et al. [13] which involves recycling of both mean and fluctuation velocities and strongly relies upon the scaling laws of the zero pressure gradient boundary layer.

The quantity $\left[u'(y)\right]_2$ in (2), strictly speaking, should be defined as

$$\left[u'(y)\right]_2 = \left[u_{LES}(y)\right]_2 - < \left[u_{LES}(y)\right]_2 >, \tag{3}$$

where $< \left[u_{LES}(y)\right]_2 >$ is the time averaged LES solution in the recycling section. However time averaging is, first, computationally expensive and, second, tangibly complicates the algorithm. It is also inadequate in quasi-steady flows. So we prefer the following approximate definition of the fluctuations in the recycling section, relying upon the available RANS solution in this section:

$$\left[u'(y)\right]_2 = \left[u_{LES}(y)\right]_2 - \left[u_{RANS}(y)\right]_2 . \tag{4}$$

This definition introduces an "error" equal to the difference between the time-averaged LES and RANS solutions $< \left[u_{LES}(y)\right]_2 > - \left[u_{RANS}(y)\right]_2$. Considering that the recycling procedure has a positive feedback as the boundary-layer thickness propagates from Section 1 to Section 2, this error may increase in the course of simulation. This should be prevented, which is ensured by a proper definition of the scaling coefficient α given in Section 2.3 after first presenting the wall-normal coordinate transformation function $\beta(y)$.

2.2 Wall-normal coordinate transformation function $\beta(y)$

This transformation is needed to account for the downstream flow evolution, typically a thickening of the boundary layer (a strong favourable pressure gradient would create an opposite trend). In the proposed approach the scaling factor is defined based on the evolution of turbulent kinetic energy profiles in the inflow and recycling sections from the RANS solution, which is available in the RANS-LES overlapping region. Generally speaking, this requires a two-equation model but a version based on the eddy viscosity is also viable.

A typical RANS-profile of the kinetic energy in a boundary layer is shown in Fig. 2. In order to define the transformation function $\beta(y)$, we divide this profile into two sub-domains: an "energy containing" one ($0 \le y \le y_a$, "region A" in the figure) extending roughly to the edge of the boundary layer and a "tail" one ($y \ge y_a$, "region B"). The boundary between the two sub-domains, $y = y_a$, is defined as the point, at which the ratio of two integrals, $I_2 = \int_{y_a}^{y_2} k(y)\,dy$ and $I_1 = \int_{y_{\max}}^{y_a} k(y)\,dy$, is equal to a prescribed small value ε. The limits of the integrals, $y_{\max}$ and y_2 are, respectively: the coordinate of the maximum of the k-profile and of the point which is twice as far from $y_{\max}$ as y_a is, if such a point exists within the computational domain, or otherwise, the boundary of the domain, y_B: $y_2 = \min\left\{\left[y_a + (y_a - y_{\max})\right],\ y_B\right\}$. Based on numerical experiments, the value of ε is set equal to 10^{-3}. With this value the width of the energy-containing part of the kinetic energy profile y_a turns out to be close to the boundary-layer thickness. However, this definition is more reliable than conventional definitions of the boundary layer thickness, since it does not depend on subtleties of the behaviour of the velocity profile in the outer part of the computational domain (typically due to curvature or shock waves).

Returning to the function $\beta(y)$, let us consider the RANS kinetic energy profiles in the LES-inflow and recycling sections of the flow (solid and dashed curves respectively in Fig. 3). The simplest possible way to define β in the near-wall

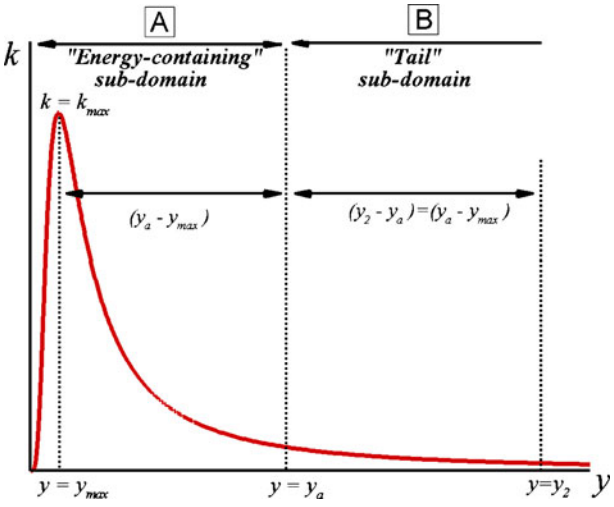

Fig. 2 Typical profile of turbulent kinetic energy in a boundary layer and its two sub-domains

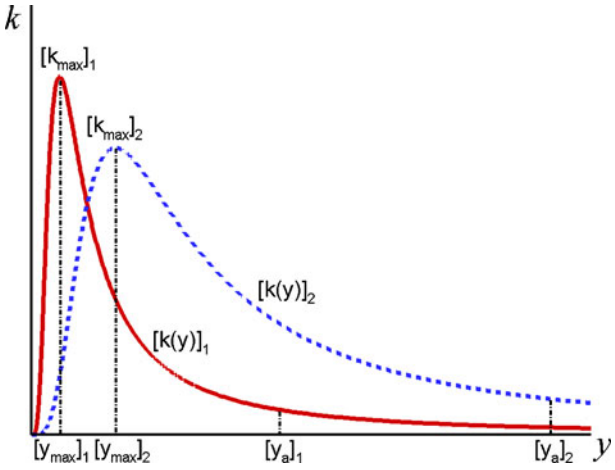

Fig. 3 Typical profiles of turbulent kinetic energy at the LES inflow and recycling sections and quantities used in the computation of the transformation function $\beta(y)$

boundary layers is to keep it independent of y and to compute it as the ratio of the widths of the energy-containing sub-domains of the two profiles:

$$\beta = \left[y_a\right]_1 / \left[y_a\right]_2 . \tag{5}$$

Although this is rather crude approach (strictly speaking β should be defined differently for the inner and outer parts of the boundary layer [13]), as shown in [14], the performance of the simplified approach without accounting for the difference between the inner and outer scaling laws turns out to be more than acceptable. Nonetheless, we prefer to use another approach, which ensures a more accurate reproduction of the shape of the kinetic energy profile. It assumes that the energy containing parts ($0 < y < y_a$) of the k-profiles in the LES-inflow and recycling sections have only one maximum. In this case β can be computed separately for the left ($0 < y < y_{\max}$) and right ($y_{\max} < y < y_a$) parts of the profiles. Below the procedure is illustrated as applied to the right part.

We first normalize the k-profiles as follows:

$$\bar{k}\,(y) = \left[k\,(y) - k_{\min}\right] / \left(k_{\max} - k_{\min}\right), \tag{6}$$

where, as earlier, $k_{\max} = k\,(y_{\max})$, whereas $k_{\min} = k\,(y_a)$.

Then, for a given value of the wall-normal coordinate in Section 1, $y = y_1$, we define $\beta_{right}(y_1)$ as the ratio y_1/y_2, where y_2 is the value of the wall normal coordinate in Section 2 at which

$$\bar{k}_2\,(y_2) = \bar{k}_1\,(y_1) . \tag{7}$$

As a result, we get the following relation for transformation of the normalized kinetic energy profile:

$$\bar{k}_1\,(y) = \bar{k}_2\left[y/\beta_{right}\,(y)\right], \tag{8}$$

The definition of the wall-normal coordinate transformation function $\beta_{left}(y)$ in the left part of the k-profile in Section 1, i.e., at $0 < y < y_{\max}$ is exactly the same as that of the function $\beta_{right}(y)$ outlined above, while in the remaining, or tail, part of the k-profile ($y > y_a$), β is set equal to its value at point a, i.e., $\beta\,(y > y_a) = \beta\,(y_a)$.

Note that if the normalized k-profiles in the two sections can be mapped from each other by a simple constant stretching, i.e., when $\bar{k}_1(y) = \bar{k}_2(y/\beta_0)$, $\beta_0 = const(y)$, then both definitions of $\beta(y)$ described above return the same value equal to β_0.

The most general possible way of defining β, which is applicable to k-profiles of arbitrary shape (with multiple maximums within the energy-containing part) and, in addition, does not involve an accurate computation of the quantities $k_{\max}$ and $y_{\max}$, is based on the integral form of (7), i.e., on the definition of y_2 as the value of y in Section 2 at which the following relation holds

$$\frac{\int_0^{y_2} k_2(y)\,dy}{\int_0^{[y_a]_2} k_2(y)\,dy} = \frac{\int_0^{y_1} k_1(y)\,dy}{\int_0^{[y_a]_1} k_1(y)\,dy}. \tag{9}$$

Note that in the case of a constant-stretching transformation $\bar{k}_1(y) = \bar{k}_2(y/\beta_0)$, this relation reduces to (7) and again results in $\beta(y) = \beta_0$.

Considering that in the specific flow computed in the present work the RANS k-profiles have only one maximum, the simulations presented in Sections 3, 4 are carried out with the use of the definition of $\beta(y)$ based on (7). However, it was checked that at least for a ZPG BL, the more general integral definition based on (9) gives very close results.

2.3 Scaling coefficient α

In order to define this coefficient we posit that the recycling formula (2) should ensure continuity of the integral of the turbulent kinetic energy averaged over some distance in the spanwise direction at the RANS-LES interface (Section 1). Moreover, we suppose that this should be ensured separately within the energy-containing and "tail" parts of the RANS k-profile defined above (see Fig. 2), that is, the following relations should be satisfied

$$\int_{z_0-l_z}^{z_0+l_z}\int_{y_1}^{y_2} \left[k^{res}_{LES}(y,\,z)\right]_1 dydz = \int_{z_0-l_z}^{z_0+l_z}\int_{y_1}^{y_2} \left(\left[k_{RANS}(y,\,z)\right]_1 - \left[k^{\,\mathrm{mod}}_{LES}(y,\,z)\right]_1\right) dydz, \tag{10}$$

where y_1 and y_2 are the ends of either the energy-containing ($y_1 = 0$, $y_2 = y_a$), or the tail ($y_1 = y_a$, $y_2 = y_B$) sub-domains of the k-profile in the Section 1.

The quantity $\left[k^{res}_{LES}(y,\,z)\right]_1$ in (10) is the resolved turbulent kinetic energy from LES at any spanwise location z:

$$\left[k^{res}_{LES}(y,\,z)\right]_1 = \frac{1}{2}\left\{\left[u'(y,\,z)\right]_1^2 + \left[v'(y,\,z)\right]_1^2 + \left[w'(y,\,z)\right]_1^2\right\}, \tag{11}$$

where the velocity fluctuations are defined by (2). The quantities $\left[k_{RANS}(y,\,z)\right]_1$ and $\left[k^{\,\mathrm{mod}}_{LES}(y,\,z)\right]_1$ are the modelled turbulent kinetic energies from RANS and LES, respectively. Finally, the length of span-averaging, l_z, is same for both sub-domains of the k-profile and, based on preliminary numerical experiments, should be of the order of the width of the energy-containing part of the k-profile y_a (i.e., of the order of the boundary-layer thickness).

After a substitution of (2) into (10), (11), we arrive to the following relation for the scaling coefficient α

$$\alpha^2 = \frac{\int\limits_{z_0-l_z}^{z_0+l_z}\int\limits_{y_1}^{y_2}\left(\left[k_{RANS}\left(y,\ z\right)\right]_1 - \left[k_{LES}^{\mathrm{mod}}\left(y,\ z\right)\right]_1\right)dydz}{\int\limits_{z_0-l_z}^{z_0+l_z}\int\limits_{y_1}^{y_2}\frac{1}{2}\left\{\left[\tilde{u}'\left(y,z\right)\right]_1^2 + \left[\tilde{v}'\left(y,z\right)\right]_1^2 + \left[\tilde{w}'\left(y,z\right)\right]_1^2\right\}dydz} \tag{12}$$

where the quantities with tilde defined as

$$\left[\tilde{u}'\left(y,z\right)\right]_1 = \left[u'\left(y/\beta,z\right)\right]_2, \left[\tilde{v}'\left(y,z\right)\right]_1 = \left[v\left(y/\beta,z\right)\right]_2, \left[\tilde{w}'\left(y,z\right)\right]_1 = \left[w'\left(y/\beta,z\right)\right]_2 \tag{12a}$$

can be viewed as preliminary estimates of the velocity fluctuations at the RANS-LES interface obtained from (2) at $\alpha = 1$.

To complete the definition of α we have yet to specify the turbulent kinetic energy from RANS $\left[k_{RANS}\left(y,\ z\right)\right]_1$ and the modelled part of the kinetic energy from LES $\left[k_{LES}^{\mathrm{mod}}\left(y,\ z\right)\right]_1$ in Section 1 which are involved in (12).

As far as $\left[k_{RANS}\left(y,\ z\right)\right]_1$ is concerned, it is either directly available from the RANS solution or, if the turbulence model used does not involve it (e.g., the Spalart-Allmaras model [15]), is computed as

$$k = \left(\nu_t\right)_{RANS} S/c_\mu^{1/2}, \tag{13}$$

where $\left(\nu_t\right)_{RANS}$ is the RANS eddy viscosity, S is the strain magnitude, and $c_\mu = 0.09$.

The definition of $\left[k_{LES}^{\mathrm{mod}}\left(y,\ z\right)\right]_1$ depends on the Sub-Grid Scale (SGS) model used in LES. In the examples presented in Sections 3 and 4 we couple RANS not with a pure LES but with a recent enhancement of the Delayed Detached Eddy-Simulation (DDES) [16] proposed in [17] and named Improved DDES (IDDES). It couples DDES with another RANS-LES hybrid model aimed at WMLES so that the performance of the combined model depends on whether the simulation does or does not have inflow turbulent content. In the case with turbulent content considered in the present study, IDDES reduces to its WMLES branch. The latter resolves most of the turbulence, within the capabilities of the grid and, as shown in [17], provides a decisive increase of the resolved turbulence activity near the wall thus adjusting the resolved logarithmic layer to line up with the modelled one, i.e., removing the "log layer mismatch", which is common in DES [7] and other WMLES methods [3, 4].

Considering that the SGS model used in IDDES is based on the S-A eddy viscosity model, the algorithm used in the present study for computing the quantity $\left[k_{LES}^{\mathrm{mod}}\left(y,\ z\right)\right]_1$ in (12) at the inflow section of the IDDES domain relies upon the evaluation of the eddy viscosity at this section, $\left[\left(\nu_t\right)_{IDDES}\right]_1$, with the use of the following relation:

$$\left[k_{LES}^{\mathrm{mod}}\left(y,\ z\right)\right]_1 = \left[\left(\nu_t\right)_{IDDES}\right]_1 \left[S_{IDDES}\right]_1 /c_\mu^{1/2}, \tag{14}$$

where $\left[S_{IDDES}\right]_1$ is the instantaneous strain magnitude from the IDDES at the previous time step of the simulation.

The quantity $\left[(\nu_t)_{IDDES}\right]_1$, in turn, is obtained from the RANS and SGS eddy viscosities by the following empirical blending, similar to that used in IDDES for the hybrid, RANS-LES, length scale (see [17] for details):

$$(\nu_t)_{IDDES} = \tilde{f}_B\, f_{corr}\, (\nu_t)_{RANS} + \left(1 - \tilde{f}_B\right) (\nu_t)_{LES}\,. \tag{15}$$

Here $(\nu_t)_{LES}$ is the SGS eddy viscosity computed with the use of the algebraic Smagorinsky model

$$(\nu_t)_{LES} = (0.2\Delta_{LES})^2\, S. \tag{16}$$

The empirical blending function $\tilde{f}_B\,(d_w/h_{\max})$ is defined as

$$\tilde{f}_B = \exp\left[-(1.1 d_w/h_{\max})^6\right] \tag{17}$$

and is close to the blending function f_B from [17].

Finally, the SGS length-scale Δ_{LES} in (16) is given by [17]:

$$\Delta_{LES} = \min\left\{\max\left[C_w d_w,\ C_w h_{\max},\ h_{wn}\right],\ h_{\max}\right\},\ C_w = 0.15, \tag{18}$$

and $h_{\max}$ and h_{wn} are the maximum and wall-normal steps of the grid.

As far as the function f_{corr} in (15) is concerned, it is introduced to ensure a fine adjustment of the RANS branch of $(\nu_t)_{IDDES}$ to the actual IDDES eddy-viscosity profile. This function, designed based on the results of IDDES of the ZPG BL, reads as:

$$f_{corr} = \exp\left[-2.5 d_w/h_{\max}\right]. \tag{19}$$

Figure 4 presents an example of the eddy-viscosity profile in the ZPG BL (see Section 3 below) at the RANS-LES interface obtained with the use of (15). Its similarity with the "developed" $(\nu_t)_{IDDES}$ profile at the boundary layer section $x = 4$ also shown in the figure and with the ν_t profiles from IDDES of developed channel flow (see [4, 17]) confirms that the approximate evaluation of $(\nu_t)_{IDDES}$ at the inlet of the IDDES domain described above indeed provides a realistic representation in the whole boundary layer. Note also that the behaviour of $(\nu_t)_{IDDES}$ in the close vicinity

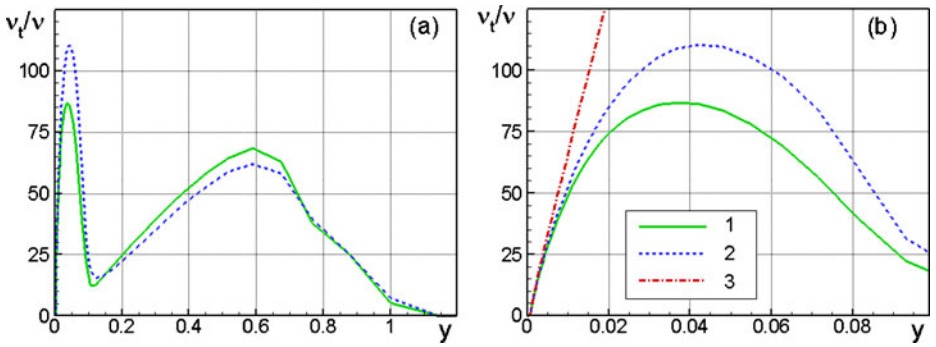

Fig. 4 Eddy/SGS viscosity profiles at RANS/LES interface and in the "developed" IDDES section of a ZPG BL (**a**) and their zoomed fragment near the wall (**b**): 1–$(\nu_t)_{IDDES}$ at the interface ($x = 1$) obtained from (15); 2–$(\nu_t)_{IDDES}$ at $x = 4$; 3–$(\nu_t)_{RANS}$ at $x = 1$

of the wall is the same as that of the S-A RANS eddy viscosity (see Fig. 4b). This is the norm with wall modelling.

Finally, considering that the piece-wise computation of the scaling coefficient α (12) results in a discontinuity at the boundary of the sub-domains A and B of k-profile (see Fig. 2), the following simple linear "smoothing" of α is applied in the energy-containing part of the profile near this boundary:

$$(\alpha_A)_{smooth} = f\alpha_A + (1 - f)\,\alpha_B,\ f = \min\{10\,(1 - y/y_a)\,,\ 1\}\,. \tag{20}$$

Note in conclusion that at the inflow of the IDDES domain and outflow of the RANS domain, variables other than the velocity components (namely, the pressure and temperature) are obtained with the use of the standard inter-block boundary conditions for overlapping grids.

The recycling procedure outlined above is summarized in the Appendix.

3 Tests of the Recycling Algorithm

To assess the performance of the new recycling algorithm, it has been applied to two flows, the ZPG BL and the flow over the A-airfoil at 13.3° angle of attack, which was studied experimentally in [18] and used for validation of LES (see [19, 20]). In this section we present results of these two tests, carried out with the SA-based version of IDDES. The simulations are performed with the incompressible branch of the NTS code [21], which runs on structured overlapping multiblock curvilinear grids with the implicit 2nd order in time (with dual time-stepping) scheme of Rogers and Kwak [22]. The viscous terms are approximated with second-order central differences, whereas for the inviscid fluxes, a 3rd-order upwind-biased scheme is used in the RANS domain and a 4th-order centered scheme in the IDDES domain.

In both cases the turbulent content in the IDDES region needed to initialize the simulations was specified by imposing velocity fluctuations obtained from LES of isotropic homogeneous turbulence with the use of the subgrid version of the S-A model as described in [16] on the RANS velocity field. The simulations rapidly recover from this rather unrealistic initial field.

3.1 Zero pressure gradient boundary layer

Simulations were performed at a Reynolds number based on the boundary layer thickness at the inflow boundary, δ_0, equal to 50,000. The grid and RANS and IDDES domains used in the simulations are shown in Fig. 5.

The grid in the wall-normal direction was built in accordance with general rules for the viscous sublayer resolving approaches, i.e., the near wall y-step in the wall units was less than 1.0. The wall-parallel grid steps, Δx and Δz, were uniform and equal to $\delta_0/10$ and $\delta_0/20$ respectively, which is also consistent with a generally accepted WMLES practice (corresponding values of the wall-parallel steps in the wall units at the inflow of the domain are about 1600 and 800, and therefore far in excess of wall-resolved LES values). The span size of the domain is $3\delta_0$. In order to get an idea of the sensitivity of the results to the recycling length l_{rec}, a series of simulations was carried out with different l_{rec} values.

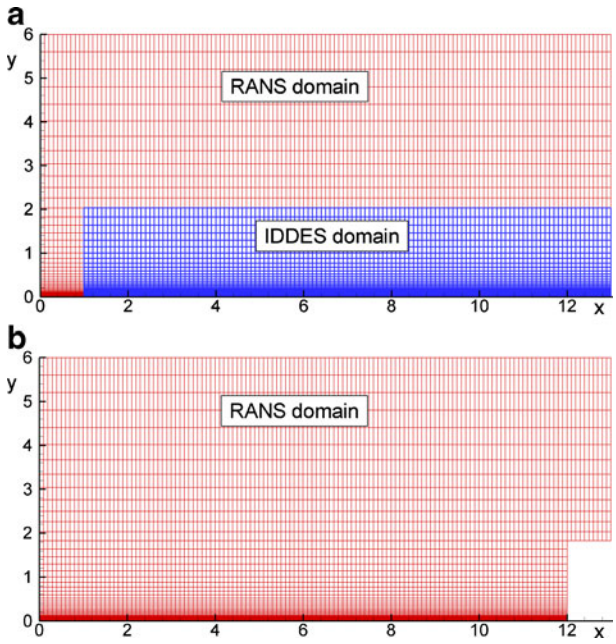

Fig. 5 Computational domain and grid in the XY-plane used in simulations of ZPG BL. **a** RANS and IDDES domains; **b** RANS domain only

Figure 6 gives a general idea about the resolution of the vortical structures provided by the newly developed approach with the length of the recycling section set at $l_{rec} = 6\delta_0$. It suggests that, indeed, the recycling procedure provides a successful injection of turbulence right at the inlet of the IDDES domain, and a qualitatively correct development farther downstream. However, as seen in Figs. 7, 8, where the vorticity snapshots are presented in an XY- and in two XZ-planes of the

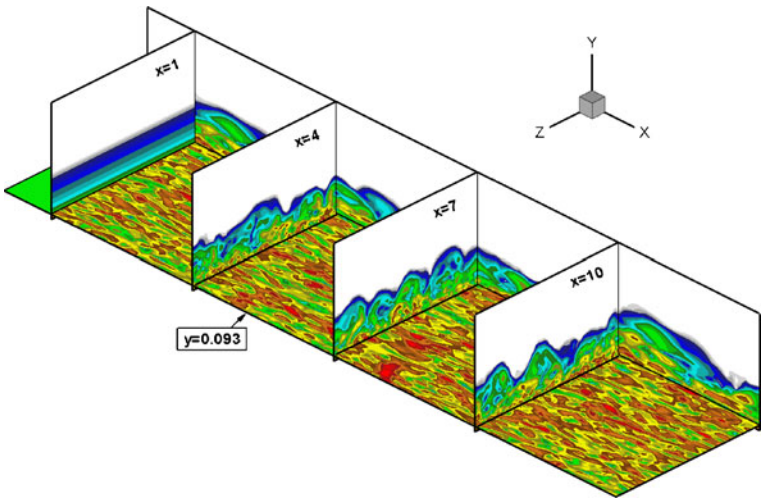

Fig. 6 Instantaneous field of vorticity magnitude from simulation of ZPG BL at $l_{rec} = 6\delta_0$

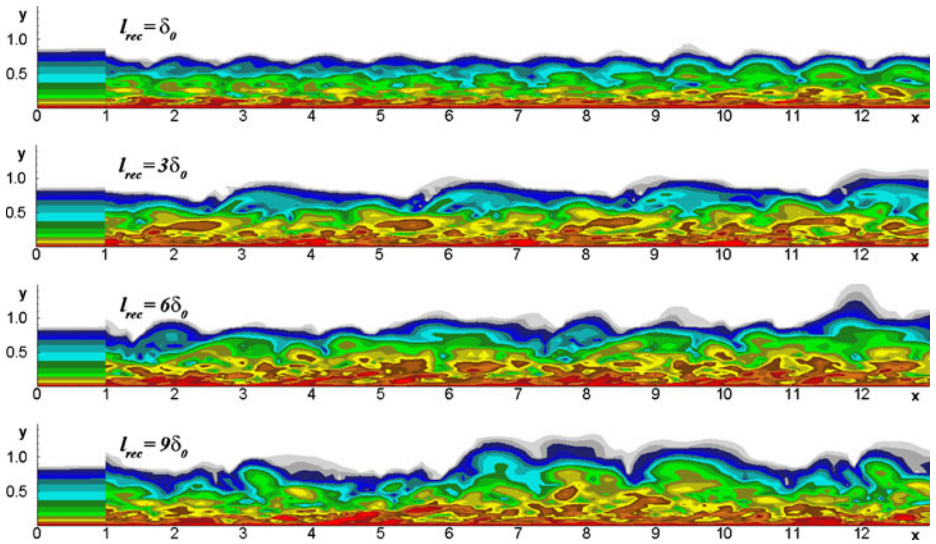

Fig. 7 Effect of recycling length on instantaneous fields of vorticity magnitude in the XY-plane of ZPG BL

boundary layer, the character of the turbulence evolution depends on the value of l_{rec}. In particular, the figures clearly show that too short a recycling length results in the appearance of a spurious frequency, which manifests itself in a streamwise modulation of the flow parameters with a wavelength close to l_{rec}. This modulation is more visually pronounced in the outer part of the boundary layer (compare left and

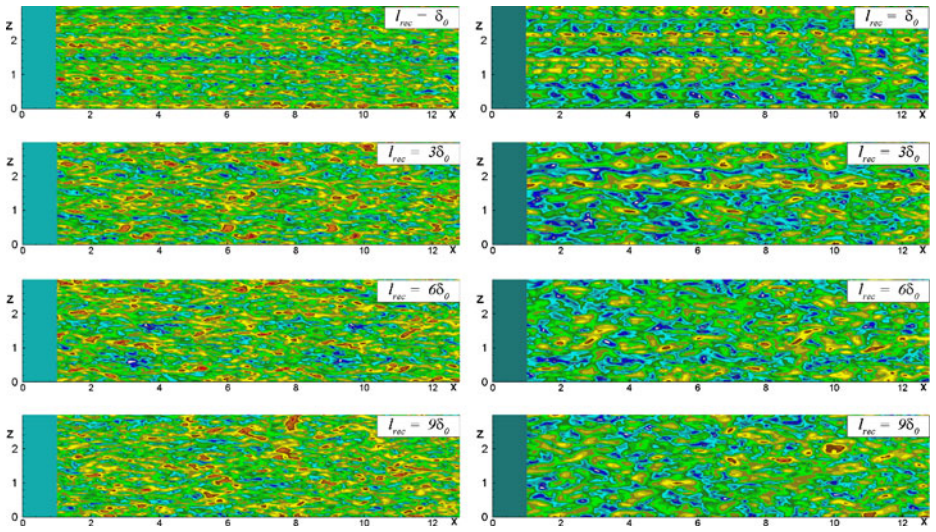

Fig. 8 Effect of recycling length on instantaneous fields of vorticity magnitude in the XZ-plane of ZPG BL. *Left* $y = 0.1$ ($y^+ = 1,600$); *right* $y = 0.4$ ($y^+ = 6,400$) Q2

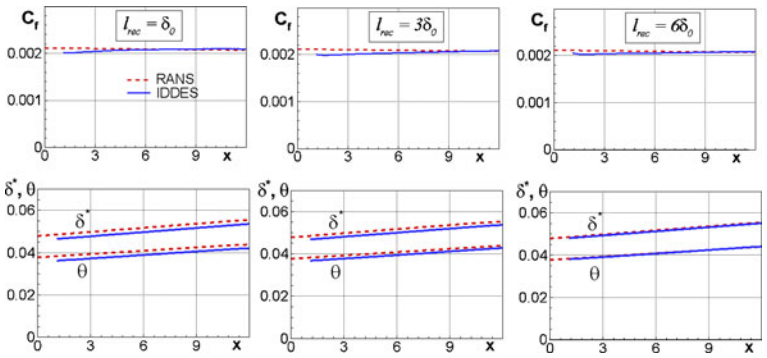

Fig. 9 Effect of recycling length on streamwise distributions of wall friction coefficient (*upper row*) and displacement and momentum thicknesses of ZPG BL (*lower row*)

right columns of Fig. 8). Other than that, the vorticity fields in the XZ-planes clearly reveal regular "trains" of vortices at constant z values, which are also associated with the excessively short recycling length. However, as seen from Fig. 8 and, also, from Figs. 9, 10, where the streamwise evolution is shown of the mean flow parameters, these deficiencies decrease when l_{rec} increases and virtually disappear or, at least, are not visually pronounced any more already at $l_{rec} = 6\delta_0$. In particular, Fig. 9 suggests that at this value of l_{rec} the mean skin-friction and integral thicknesses of the boundary layer become almost perfect (here we consider the RANS solution also shown in the figure as the standard), although a minor discontinuity of the skin-friction at the RANS-IDDES interface still exists, and C_f in the IDDES domain is slowly growing rather than decreasing, as it should be. Other than that, as seen in Fig. 10, which compares the mean velocity and turbulent shear stress profiles from the RANS-IDDES computation at $l_{rec} = 6\delta_0$ plotted in wall units with the corresponding RANS profiles, the IDDES shear stress at the IDDES inflow (at $x/\delta_0 = 1.0$) has a "dent" at $y^+ \approx 700$, and farther downstream the stress deviates somewhat from a constant value in the log-layer (it grows and reaches a maximum at y^+ about 3×10^4). As a result, the velocity profiles have a small "bump" at this y^+. These deficiencies are probably caused by a transition from the SA RANS solution

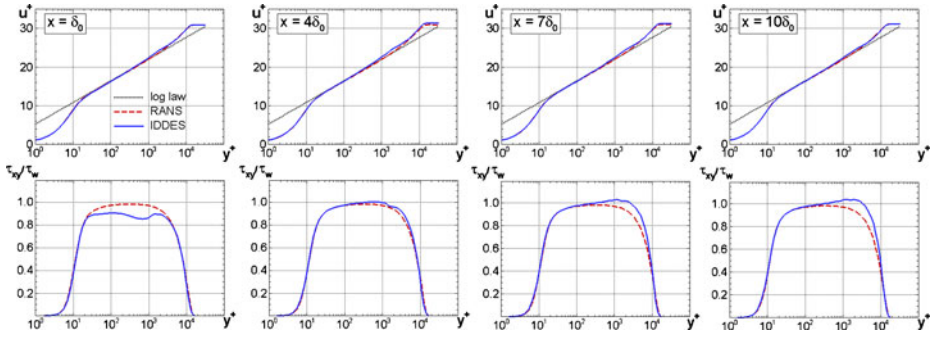

Fig. 10 Mean velocity (*upper row*) and turbulent shear stress (*lower row*) profiles from RANS and IDDES of ZPG BL in different flow sections obtained at $l_{rec} = 6\delta_0$

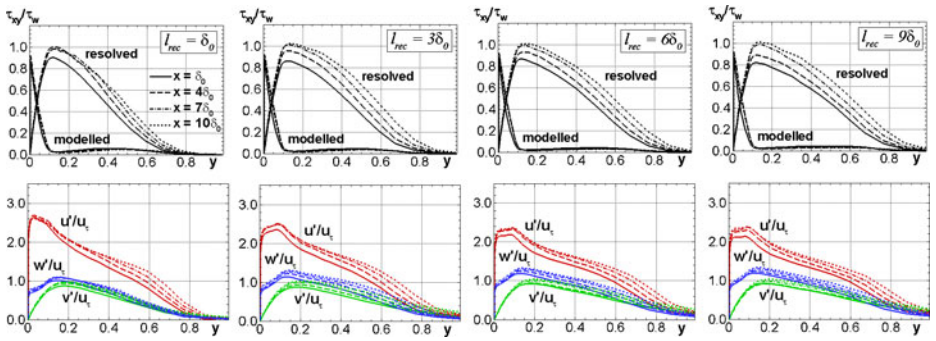

Fig. 11 Effect of recycling length on downstream evolution of modelled and resolved shear (*upper row*) and normal (*lower row*) stresses from simulation of ZPG BL

to the SA-IDDES one, which are of course not identical even for the ZPG BL, and the results obtained suggest that the relaxation period is rather long. A simple rule for a boundary layer to recover from a perturbation has been that it takes about $10\delta_0$.

Finally, Fig. 11 illustrates the effect of the recycling length on the evolution of profiles of the resolved and modelled turbulent stresses. One can see that similarly to what is observed for the mean flow, the effect is not significant and there is a clear trend to saturation with l_{rec} increasing. In particular, the difference between the profiles computed with $l_{rec} = 6\delta_0$ and $l_{rec} = 9\delta_0$ is negligible whereas the corresponding difference between the predictions obtained with $l_{rec} = 3\delta_0$ and $l_{rec} = 6\delta_0$ is noticeable, although not large.

Thus, in general, the results of the ZPG BL test of the new recycling procedure are quite satisfactory.

3.2 A-Airfoil at 13.3° angle of attack

This flow is characterized by a strong adverse pressure gradient, resulting in a thick boundary layer and shallow separation near the airfoil trailing edge. A pure RANS of such flows is believed to be somewhat inaccurate, keeping experimental

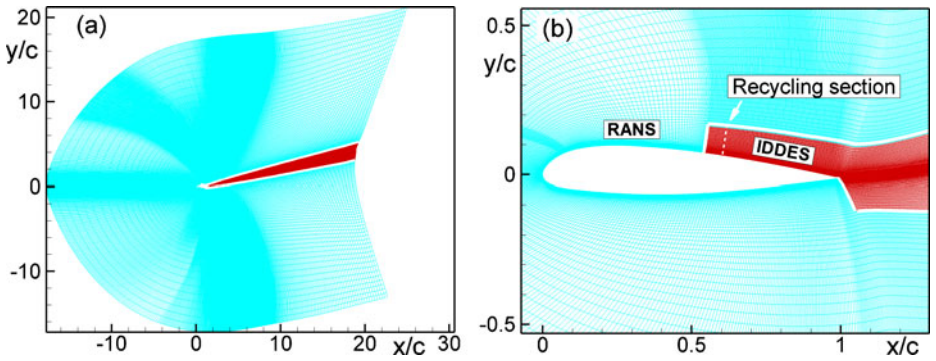

Fig. 12 Full view (**a**) and zoomed fragment (**b**) of grid in the XY-plane used in A-airfoil simulations

imperfections in mind, whereas a pure LES of the whole airfoil with sufficient lateral domain size was found far from affordable in the course of the European project LESFOIL around 2002 [19]. Thus the flow presents a good test of the proposed procedure for coupling RANS with IDDES. Recycling in a pressure gradient, even a mild one, adds difficulty and is out of reach of the method of Lund et al. [13], for instance.

Figure 12 shows the grid used in the simulation. The wall-normal step is clustering near the wall so that its near-wall value in wall units is not higher than 1.0. The step in the streamwise direction in the major part of the RANS domain is about $0.01c$, while in the IDDES domain it is $0.002c$. The span-size of the domain is equal to$10\%c$, which is an order of magnitude larger than that used in the course of the LESFOIL project, and the spanwise grid is uniform with $\Delta z = 0.001c$. The inflow section of the IDDES domain and recycling section on the suction side of the airfoil are located at $x/c = 0.54$ and 0.6 respectively so that the length of the recycling zone is equal to about $3\delta_0$(δ_0 being the boundary layer thickness at $x/c = 0.54$). On the pressure side, the inflow of the IDDES region is set at $x/c = 1$ (right at the trailing edge) and no recycling is applied there. Preliminary simulations have shown that applying the recycling procedure on the pressure side as well requires a significant increase of the total grid count because of the thin boundary layer there and does not result in any visible alteration of the solution on the suction side, which we are most concerned with.

The simulation was carried with tripping the boundary layer (in the sense of the SA model). The trip on the suction side of the airfoil was set in the beginning of the separation bubble in the experiment ($x_{trip}/c = 0.08$) and on the pressure side, at the transition point known from the experiment ($x_{trip}/c = 0.3$).

Figure 13 gives a general idea of the performance of the recycling procedure and suggests, in particular, that similarly to what was observed in the ZPG BL, the procedure ensures a rapid development of resolved turbulence at the RANS-IDDES interface. The figure shows also that the simulation resolves rather fine turbulent structures in the boundary layer on the suction side and in the near-wake of the airfoil, whereas farther downstream, consistently with the coarsening of the grid in this region, only relatively large structures are resolved. Also, the flow visualization shows some delay of forming turbulent structures in the lower part of the wake caused by the absence of turbulent content at the inflow of IDDES at the pressure

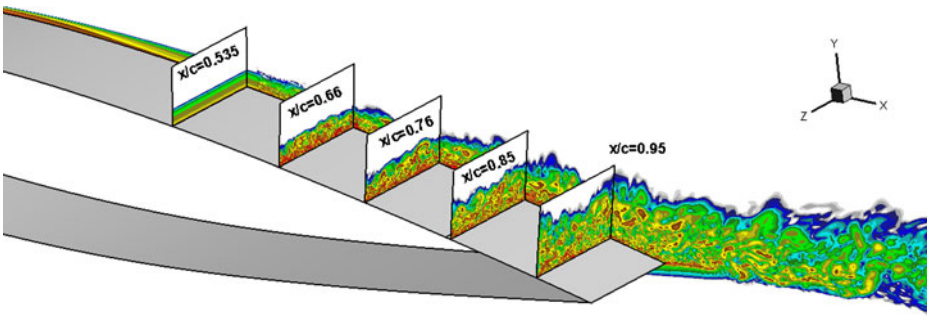

Fig. 13 Instantaneous field of vorticity magnitude from simulation of A-airfoil flow

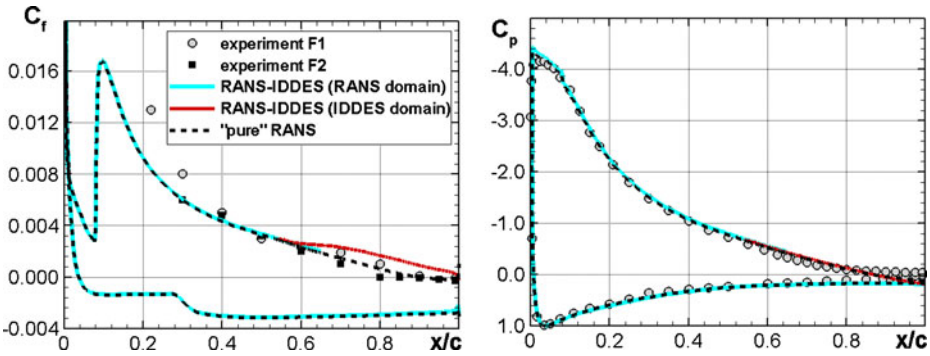

Fig. 14 Comparison of RANS-IDDES predictions of friction and pressure distributions over A-airfoil surface with experiment and "pure" RANS results

side of the airfoil. However, as mentioned above, this does not result in any alteration of the solution on the suction side.

Figure 14 presents computed mean friction and pressure distributions over the airfoil. It shows that the recycling procedure provides a smooth transition from the RANS to IDDES even for the friction coefficient and does not introduce any visible non-smoothness into the pressure distribution.

The credibility of the recycling procedure is also supported by Fig. 15, which shows that the RANS and IDDES velocity and shear stress profiles at the inlet of the IDDES domain and in the recycling section are close to each other.

Thus, as far as the recycling procedure itself is concerned, the results of the simulation of the A-Airfoil may be considered as quite encouraging.

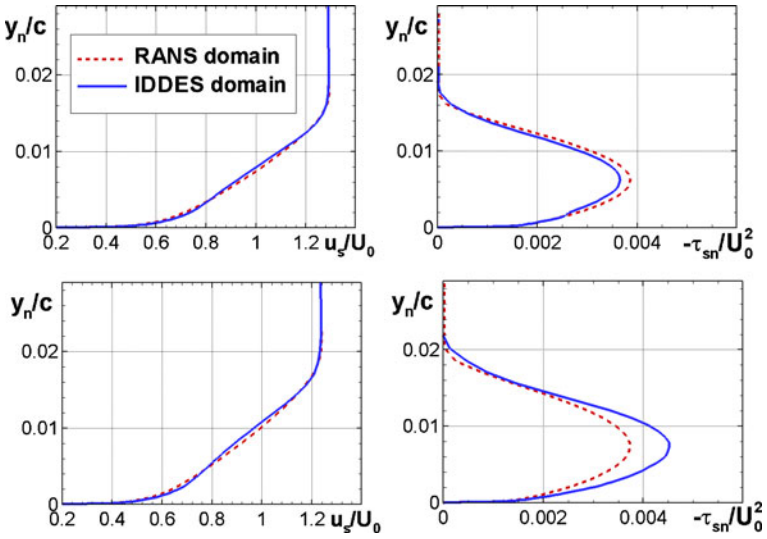

Fig. 15 Comparison of RANS and IDDES profiles of tangential velocity and turbulent shear stress at the IDDES-inflow (*upper row*) and recycling (*lower row*) sections of A-airfoil flow

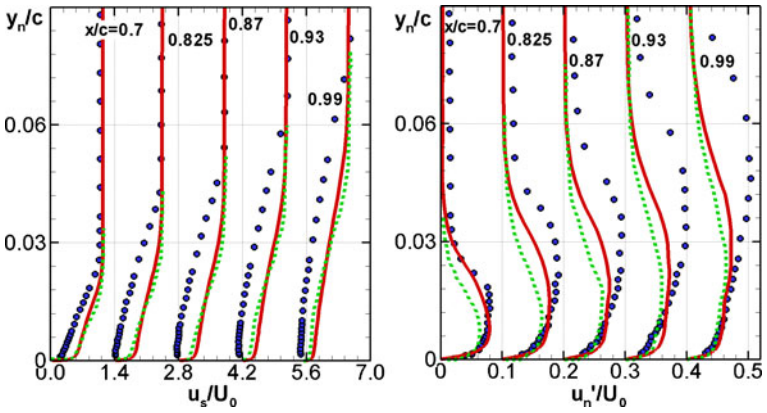

Fig. 16 Comparison of RANS-IDDES predictions of mean tangential velocity and wall-normal velocity fluctuations (*solid lines*) with experiment (*circles*) and with well-resolved LES [20] (*dashed lines*)

It is of course disappointing to observe a slight degradation of the agreement with experiment, going from RANS to IDDES. This agreement is rather poor by modern standards (see Figs. 14 and 16). The perfect solution for this flow, statistically two-dimensional and with exact mass conservation in (x, y), is not available and we speculate without strong evidence that the experimental and CFD uncertainties are now comparable. Also note that the focus of this article is on the RANS-to-IDDES change-over. A rigorous assessment of IDDES in the region of incipient separation will involve consequent grid refinement and lateral-domain enlargement, and be computationally far more expensive. In fact, quite similar results were obtained in the best available wall-resolved LES of this flow [20], which is also shown in Fig. 16.[2] Thus the disagreement may be explained by some inconsistency of the numerical and experimental set-ups, e.g., by the effect of the sidewalls of the wind tunnel which is not accounted for in the simulations. It is possible that the better CFD approaches all fall within the plausible uncertainty of the experiment, if the ideal object to be compared is a two-dimensional flow.

4 Application to Simplified Windshield Wiper Flow

Wiper blades disturb the flow at the base of windshields, and the associated turbulence contributes to cabin noise through the window. This is more pronounced on airliners than automobiles even though their glass is much thicker, because of the high dynamic pressure, smoother underlying shape, and sweep angle. The response of the glass is highly dependent on many characteristics of the pressure fluctuations

[2] A considerably better agreement of the full LES of the same flow carried out by the authors of [20] in the course of the LESFOIL project is reported in [19], but this simulation was performed in a very narrow domain in the spanwise direction (1.2% c versus 10% c in the simulations presented in Fig. 16), and so the good agreement with the data there cannot be explained other than by error cancellation.

including spectrum, spatial patterns, and propagation velocities. This motivates numerical efforts aimed at the accurate and detailed prediction of these properties, and the exploration of methodological improvements, which would take the entire chain of events into account, from the wiper to the pilot's ears. This is possible only based on turbulence-resolving approaches, capable of accurate predictions of the wall-pressure fluctuations. However a real-flight Reynolds number of 1.9×10^5 based on the wiper blade height precludes a pure LES of the flow, for cost reasons. Thus the flow presents an ideal arena for applying the coupled RANS-IDDES approach with creating IDDES inflow turbulent content, described in the previous sections.

4.1 Computational set-up and grid

The wiper system is idealized in the simulation. In particular, it includes only the wiper blade, i.e., it neglects the arm and the mechanisms attaching the blade to the arm and the arm to the wiper motor. In addition, the geometry of the blade itself does not account for subtleties of its shape nor for its finite span size, i.e., the blade is considered as an infinite rectangular obstacle, and both the upstream part of the airplane fuselage and the windshield are assumed to be flat and to have infinite extent. The specific geometry considered in the simulations (see Fig. 17) includes a blade with height $h = 0.027$ m and width $d = 0.015$ m, placed at a distance $l = 0.005$ m downstream of the edge of a 150° corner (adjacent angle $\beta = 30°$).

A key feature of this problem is that the "free stream" is not uniform but represents the compressible inviscid flow in a concave corner with a constant sweep velocity. So, in order to provide boundary conditions at the inlet and outlet boundaries of the domain we use the following approach.

Let the full Mach number (including the sweep velocity component), M_O, pressure and temperature be specified in some point "O" located on the wall, far upstream of the inlet boundary of the computational domain (Fig. 17). Then we assume that the

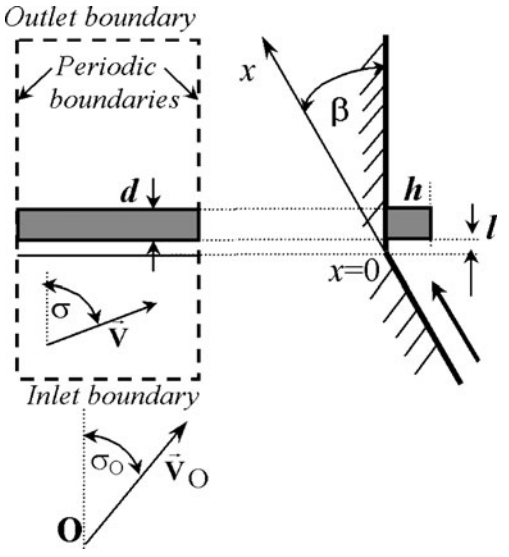

Fig. 17 Schematic of computational domain in RANS-IDDES of wiper flow

x-velocity component in this point defined by $u_O = M_O c_O \cos\sigma_O$ (c_O is the speed of sound and σ_O the sweep angle) is related to the $x-$ and y-velocity components at the free boundaries of the computational domain by the following analytical solution for the incompressible potential flow over the concave 150^o corner:

$$\frac{u_1^2 + v_1^2}{u_2^2 + v_2^2} = \left(\frac{R_1}{R_2}\right)^{\frac{2}{5}}, \frac{v}{u} = \frac{\varphi}{(180^\circ - 30^\circ)} \sin 30^\circ \tag{21}$$

where R_1 and R_2 are the radius-vectors of the arbitrary points "1" and "2" and ϕ is the polar angle.

Applying (21) for the point "O" ($u_2 = u_O$, $v_2 = 0$) and an arbitrary point Γ at the inlet or outlet boundaries of the domain, one obtains the following relations for the velocity at the boundaries:

$$\frac{u_\Gamma^2 + v_\Gamma^2}{u_O^2} = \left(\frac{R_\Gamma}{R_O}\right)^{2/5}, \frac{v_\Gamma}{u_\Gamma} = \frac{\varphi_\Gamma}{150^o} \sin 30^\circ. \tag{22}$$

Then the temperature and static pressure at the boundaries can be computed with the use of the isentropic relations using the known flow parameters in the point "O".

The velocity and temperature obtained in this manner are imposed as the boundary conditions at the inlet boundary of the domain, whereas the static pressure is specified at the outlet boundary. This is possible because the domain is large enough for the flow to reattach. For the pressure at the inlet boundary and velocity and temperature at the outlet boundary linear extrapolation from the interior of the domain is used. The eddy viscosity at the RANS inflow is set equal to the molecular one in a very close vicinity of the wall (at $y < 10^{-3}$m) and assumed to be zero at the rest of the boundary. The boundary layer is extremely thin at the RANS inflow.

Finally, at the side boundaries of the domain periodic boundary conditions are used.

In the simulations of which the results are discussed below the flow conditions are typical of a civil aircraft cruise flight, namely, at $x_O = -3$ m, $M_O = 0.85$, $\sigma_O = 30^o$, $T_O = 218$ K, $p_O = 2.25 \times 10^4$ Pa. These, as already mentioned, result in a Reynolds number based on wiper blade height equal to 1.9×10^5.

Figure 18 shows the XY-grid used in the simulations. It contains about 62,500 points, most of them located in the IDDES region (thick grid lines in the figure).

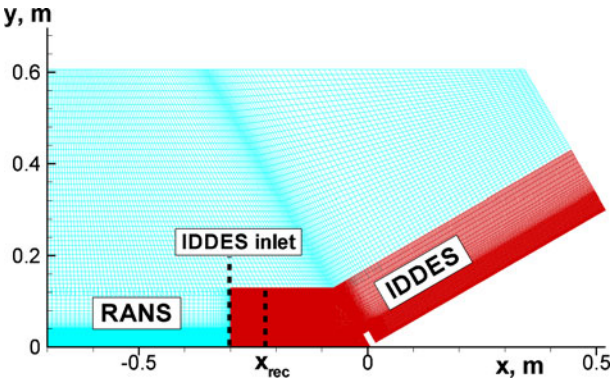

Fig. 18 Full view of grid in the XY-plane used in RANS-IDDES of wiper flow

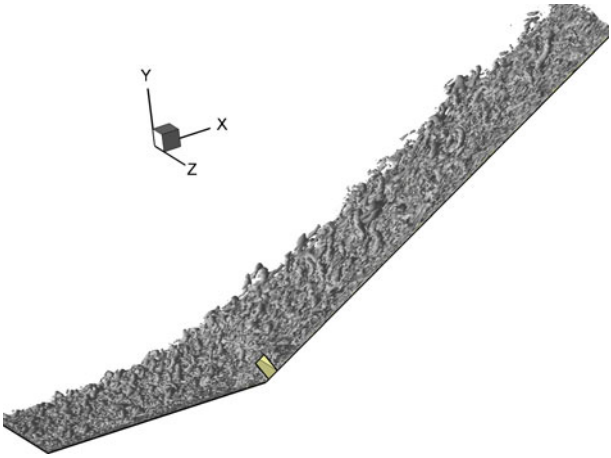

Fig. 19 Isosurface of non-dimensional (normalized with $|\mathbf{V}_O|$ and length of 1 m) swirl $\lambda = 10$ from RANS-IDDES of wiper flow at $L_z = 4h$

In the spanwise direction the grid is uniform, and the z-step is equal to $h/30$ in the IDDES region and $h/2$ in the RANS region. This can be compared with the boundary-layer thickness, which is at least $h/2$ in the IDDES region. For the two values of the period used ($L_z = 2h$ and $4h$), this results in about 4 and 8 million

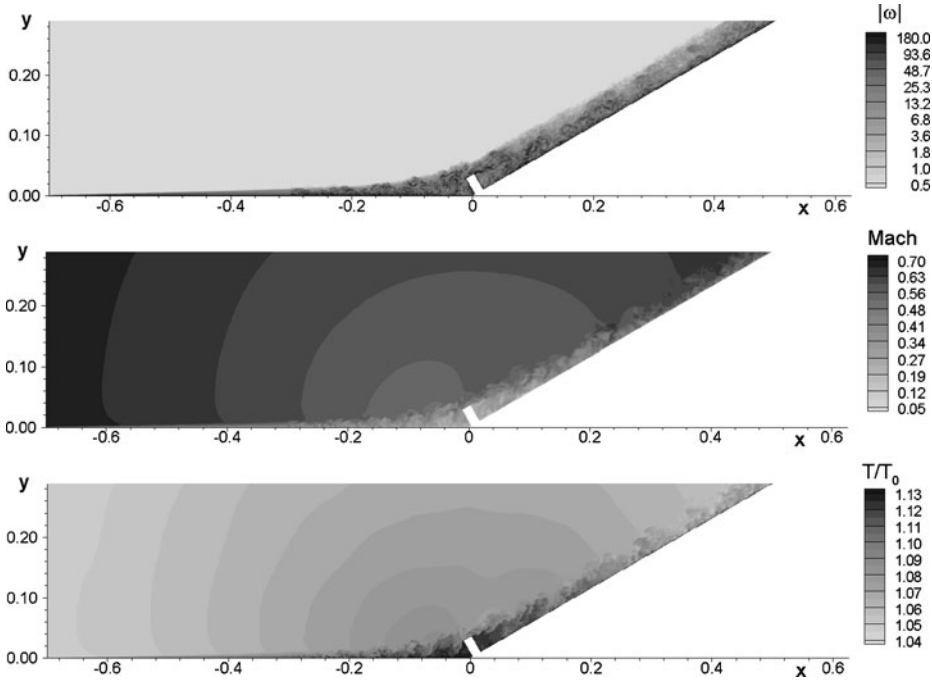

Fig. 20 Vorticity magnitude, Mach number, and temperature snapshots from RANS-IDDES of wiper flow. Vorticity is normalized with $|\mathbf{V}_O|$ and length of 1 m

nodes total respectively. The figure also shows the location of the inlet of the IDDES domain (at $x = -0.3$ m) and the position of the recycling section ($x_{rec} = -0.22$ m).

The simulations are performed with the use of the compressible branch of the NTS code [21]. In the RANS domain the differencing of inviscid fluxes is based on the third order upwind-biased flux-difference splitting scheme of Roe [23], while in the IDDES region these fluxes are approximated with the 4th order centered scheme.

4.2 Results and discussion

Figure 19, where an isosurface of the instantaneous swirl is presented from a simulation carried out in the wide ($L_z = 4\ h$) domain, gives a general idea of the turbulent structure of the flow and suggests that IDDES achieves the resolution of fine-grained turbulence even in a close vicinity of the wall.

Figure 20 presents snapshots of vorticity, Mach number, and temperature in an *XY*-plane. It does not reveal any noticeable discontinuity of the flow parameters at the RANS-IDDES interface, thus demonstrating the fine performance of the recycling procedure, and demonstrates both the "background non-uniformity" of the inviscid corner flow and the resolved turbulence in the rather thick near-wall flow region the wiper blade is immersed in.

Figure 21, where a close-up snapshot of the vorticity from Fig. 20 is drawn together with a similar eddy/SGS viscosity snapshot and with a snapshot of the vorticity magnitude on the surface, allows a more detailed evaluation of the simulation quality. One can see, in particular, that the smallest resolved turbulent structures are comparable with the size of the grid-cells in the turbulent part of the flow, which suggests that the level of numerical dissipation is acceptable. Other than that, the eddy viscosity at the RANS-IDDES interface drops abruptly by more than an order of magnitude, which allows the rapid (virtually instantaneous) triggering of

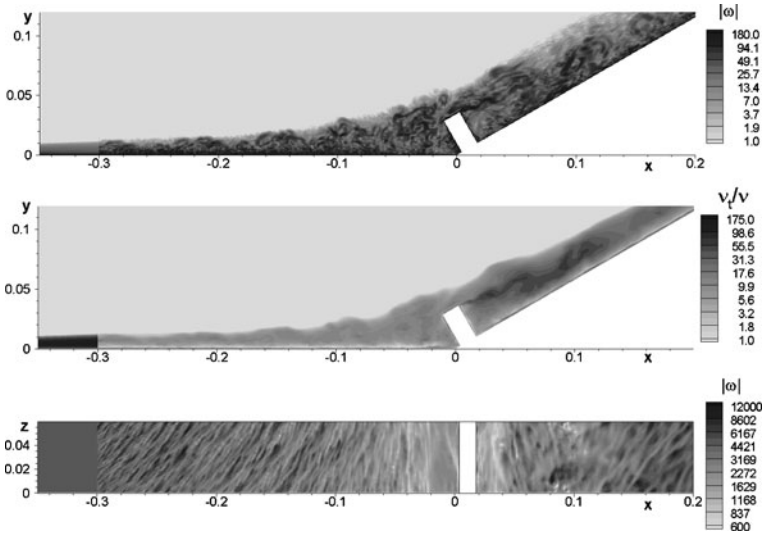

Fig. 21 Close-up views of vorticity magnitude and eddy/SGS viscosity in the XY-plane and of vorticity magnitude on the corner surface from RANS-IDDES of wiper flow

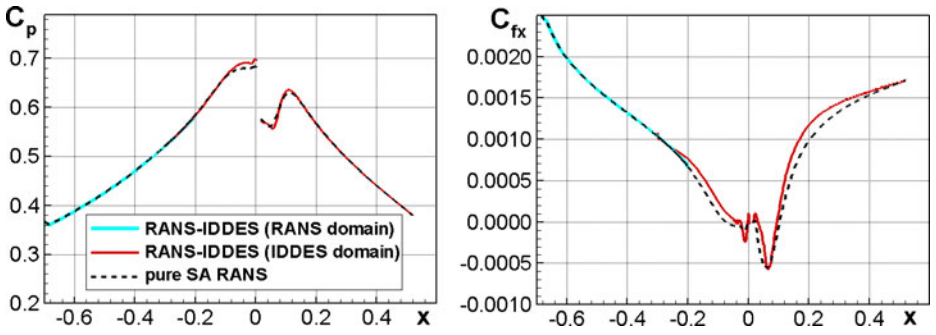

Fig. 22 Comparison of time- and span-averaged wall pressure and skin-friction distributions from RANS-IDDES with steady SA RANS predictions of wiper flow

resolved turbulence. Finally, the shape of the turbulent structures on the surface is consistent with the general knowledge about near-wall turbulence, on one hand, and with the specifics of the present flow (first of all, its strong sweep), on the other hand. Simulations without the wiper blade (not shown) have a much narrower separation bubble.

Thus, Figs. 19–21 permit to conclude that at least qualitatively both the recycling procedure, which triggers turbulent content at the RANS-IDDES interface, and the IDDES itself work properly over a non-trivial geometry.

Quantitative evidence in favour of these optimistic conclusions includes the smooth behaviour of the time- and span-averaged pressure and friction coefficients distributions at the RANS-IDDES interface and, also, a comparison of these distributions with the corresponding distributions from the steady RANS computations with the use of the SA turbulence model presented in Fig. 22. One can see that the RANS and RANS-IDDES models' predictions of the pressure are virtually identical, and that the disparity of the two friction distributions is most pronounced in the region of flow recovery after reattachment ($x > 0.1$ m), i.e., exactly in a region where the RANS model is known to predict too slow a return to standard levels of skin friction. As for the difference in the friction coefficients predicted by the two approaches upstream of the blade, it might be caused by an imperfection of the recycling procedure but may also be explained by the insufficient accuracy of RANS in the area of strong adverse pressure gradient. Finer grids and runs with other RANS models would begin to answer this question.

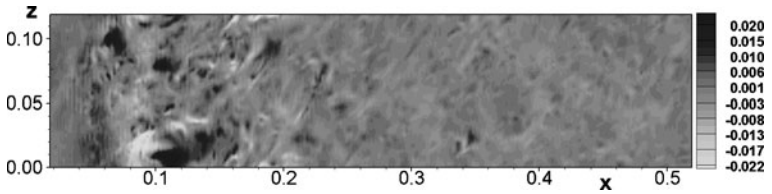

Fig. 23 Snapshot of pressure $(p - < p >) / \left(\rho_0 V_0^2\right)$ on the downstream corner wall from RANS-IDDES of wiper flow

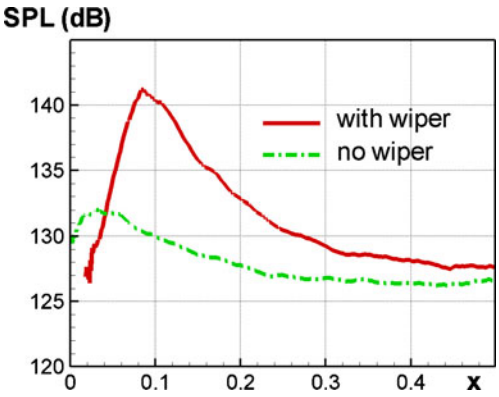

Fig. 24 Streamwise distribution of *rms* of wall pressure fluctuations from RANS-IDDES of the flow with and without wiper

Let us now consider an instantaneous pressure field on the surface downstream of the blade, presented in Fig. 23. This is the most important flow quantity in terms of evaluating the noise produced by the turbulence. The figure clearly demonstrates that the most intense turbulent fluctuations of the pressure are observed in the vicinity of the reattachment of the shear layer separated from the top of the blade. This is quantitatively supported by Fig. 24, which presents the streamwise distribution of the *rms* of the wall pressure fluctuations (in the form of the sound pressure level) with and without the blade. One can see that the effect of the blade on the SPL level is very significant and that in the flow with the blade the SPL reaches its maximum in the vicinity of the reattachment line, where it is higher than the "equilibrium" SPL by over 10 dB. The equilibrium level slightly under 130dB seems to be correct, although a little low. It may well be higher with a finer grid.

Finally, Fig. 25 presents the two-point spanwise correlations of the pressure fluctuations $R_{ij} = < p_i' p_j' > / \left(< p_i'^2 > < p_j'^2 > \right)^{1/2}$ at different streamwise locations downstream of the blade from the simulation in the wide domain $L_z = 4h$. Close to the blade (at $x = 0.05$ m) they turn out to be rather high up to the correlation length $\Delta z = 0.02$ m, but farther downstream, they drop much faster and collapse in all the considered flow sections. Thus a span size of the domain of $4h$ can be considered more than acceptable. Note that the simulation in the span domain of

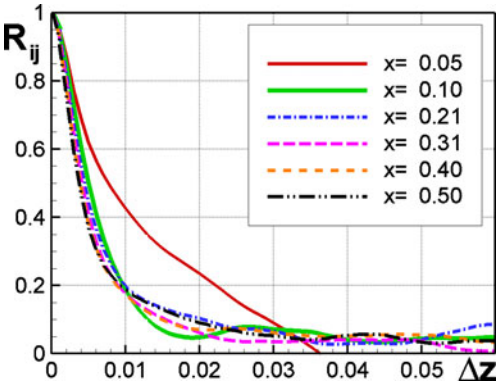

Fig. 25 Two-point spanwise correlations of wall pressure fluctuations at $L_z = 4h$ from RANS-IDDES of wiper flow

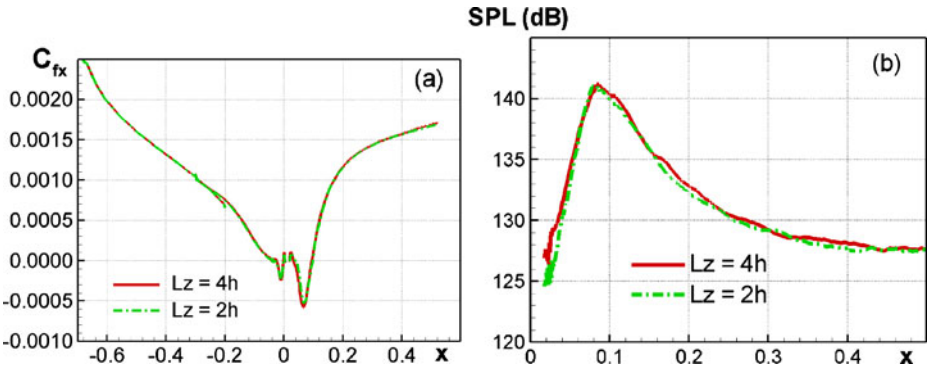

Fig. 26 Effect of span-size of domain on streamwise distribution of skin-friction (**a**) and *rms* of wall pressure fluctuations (**b**) from RANS-IDDES of wiper flow

$2h$ suggests that even this relatively small span size is quite sufficient for an accurate prediction of the mean flow characteristics and *rms* of the wall pressure fluctuations (see Fig. 26). However, the two-point correlation coefficients of the pressure do change (see Fig. 27) and remain rather high even at the largest correlation length of 0.03 m. This behaviour is not surprising considering the strong sweep of the flow right downstream of the blade: z is far from being the lateral direction locally for this flow.

Figure 28 displays an example of the "final product" of this kind of work. The wall-pressure field, $p'(x,z,t)$, is Fourier-transformed, and then the two-point correlation fields are extracted for each frequency band. In this figure, the 1/3 octave around 1200 Hz is chosen, and the first of the two points placed at $x = 0.4$ m, z = 0. The quantity is normalized with the one-point mean-square value, so that the real part, which is shown in the figure, peaks at 1 at (0.4, 0). This point is in the reattached region, where the boundary layer has largely returned to a standard state. Its thickness is about 0.04 m. The figure shows that the wall-pressure pattern is closely aligned with the wall streamlines (not shown). The pattern is also very elongated, and has the shape of a damped sinusoid in the streamwise direction, but a rapid fall to near 0 without ringing in the lateral direction. The wavelength of about 0.16 m

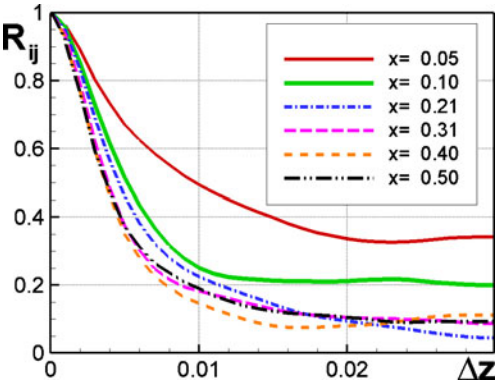

Fig. 27 Two-point spanwise correlations of wall pressure fluctuations at $L_z = 2h$ from RANS-IDDES of wiper flow

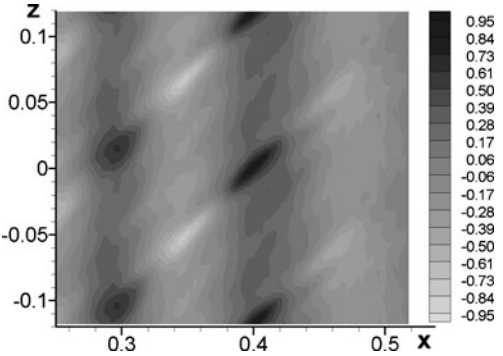

Fig. 28 Map of the 1,200 Hz 1/3-octave-passed two-point correlation coefficient based on RANS-IDDES of wiper flow; real part. $L_z = 4h$

at this frequency indicates a phase velocity of about 200 m/s, which is, as expected, about 75% of the edge velocity of the boundary layer. Finally, the differences in magnitude of the lobes for $x < 0.4$ and $x > 0.4$ reflect the slow decay of the pressure fluctuation level (Fig. 24). Qualitatively, all these features were expected.

5 Conclusions

A procedure was introduced which enables an essentially immediate switch at a chosen location from RANS, without resolved eddies, to LES, with resolved eddies carrying the Reynolds stresses in the outer part of the boundary layer. The procedure is a little involved, particularly as it rests on a double-coverage of a region of the boundary layer; as a result, it requires either a precursor RANS computation or substantial modifications to the Navier-Stokes source code. However, the motivation for it is strong, as the future of hybrid RANS-LES methods appears to include the treatment of boundary layers with LES (and usually wall modelling) upstream of separation, to the benefit of accuracy in terms of incipient separation, as well as in terms of reattachment if that is to occur. Slow recovery of the turbulence activity and late reattachment are emerging as a consistent criticism of the common RANS models. Other subtleties which outwit RANS models such as curvature, streamline convergence, shock waves, and so on, also motivate LES in attached regions. Even for massive separation, some applications will benefit from LES content flowing out with the boundary layer. This attitude does not clash with the initial motivation of Natural DES, if we observe that precisely it is here combined with pure RANS function in the thinner boundary-layer regions, the switch being imposed only after substantial thickening, which strongly softens the resolution requirements in all four directions. Figures such as 13 are convincing in that regard.

Until now, recycling methods starting with that of Lund et al. were restricted to regions without pressure gradient; the present one was demonstrated with a moderate gradient, which makes it far more general. The flows here were homogeneous in the lateral direction, but that limitation is not structural, and moderate lateral gradients may be addressed as well. Thus, the approach will be useful in specific applications, with careful design of the grid and recycling parameters. Inadequate values for these parameters have been shown capable of deteriorating the quality of the results, for instance by causing regular trains of fluctuations, but detailed flow visualisations

are always highly recommended and would reveal it. In summary, like many recent proposals in the field of complex-flow simulations, the method is somewhat delicate, but is powerful.

Acknowledgements The authors from St.-Petersburg were supported by BCA and, partially, by EC 7th Framework Programme Projects ATAAC (ACP8-GA-2009-233710) and VALIANT (ACP8-GA-2009-233680), and by the Russian Basic Research Foundation (grant No. 09-08-00126a).

Appendix: Summary of the Recycling Procedure

Here we briefly summarize the main steps of the algorithm of recycling presented in Section 2 as applied to coupled RANS-IDDES computations. At every time-step of the solution, these steps are as follows.

1. Computation of velocity fluctuations in the recycling section based on the available IDDES and RANS solutions:
$$\left[u'(y,z)\right]_2 = \left[u_{IDDES}(y,z)\right]_2 - \left[u_{RANS}(y,z)\right]_2 .$$
2. Computation of the coordinate-transformation function $\beta(y,z)$ in the IDDES-inflow section based on relations (7) or (9) with the use of the k-profiles available from RANS in the inflow and recycling sections, $\left[k_{RANS}(y,z)\right]_1$ and $\left[k_{RANS}(y,z)\right]_2$, as described in Section 2.2.
3. Computation of the preliminary estimates of velocity fluctuations in the IDDES-inflow section $\left[\tilde{u}'(y,z)\right]_1, \left[\tilde{v}'(y,z)\right]_1, \left[\tilde{w}'(y,z)\right]_1$ with the use of (12a).
4. Computation of the inflow IDDES eddy viscosity profile with the use of (15) and of the quantity $\left[k^{\mathrm{mod}}_{IDDES}(y,z)\right]_1$ in accordance with (14).
5. Calculation of the scaling coefficients α in the two sub-domains of the inflow profile with the use of (12) and application of smoothing (20) to obtain the final distributions $\alpha(y,z)$. Then the final velocity fluctuation in the IDDES inflow section, $\left[u'(y,z)\right]_1, \left[v'(y,z)\right]_1, \left[w'(y,z)\right]_1$ are computed by multiplication of the preliminary fluctuations $\left[\tilde{u}'(y,z)\right]_1, \left[\tilde{v}'(y,z)\right]_1, \left[\tilde{w}'(y,z)\right]_1$ obtained at step 3 by $\alpha(y,z)$.
6. Calculation of the final distributions of velocity components in the inflow IDDES section (they are used as the inflow boundary conditions for IDDES) as:
$$\left[u_{IDDES}(y,z)\right]_1 = \left[u_{RANS}(y,z)\right]_1 + \left[u'(y,z)\right]_1 .$$

References

1. Spalart, P.R., Jou, W.-H., Strelets, M., Allmaras, S.R.: Comments on the feasibility of LES for wings, and on a hybrid RANS/LES approach. In: Liu, C., Liu, Z. (eds.) Advances in DNS/LES, pp. 137–147. Greyden, Columbus (1997)
2. Spalart, P.R.: Detached-Eddy simulation. Annu. Rev. Fluid Mech. **41**, 181–202 (2009)
3. Piomelli, U., Balaras, E.: Wall-layer models for large-eddy simulation. Annu. Rev. Fluid Mech. **34**, 349–374 (2002)
4. Piomelli, U.: Wall-layer models for large-eddy simulation. Prog. Aerosp. Sci. **44**, 437–446 (2008)
5. Leschziner, M.A., Li, N., Tessicini, F.: Computational methods combining eddy simulation with approximate wall-layer models for predicting separated turbulent flows. ERCOFTAC Bulletin. **72** (2007)

6. Fröhlich, J., von Terzi, D.: Hybrid LES/RANS methods for the simulation of turbulent flows. Hybrid LES/RANS methods for the simulation of turbulent flows. Prog. Aerosp. Sci. **44**, 349–377 (2008)
7. Nikitin, N.V., Nicoud, F., Wasistho, B., Squires, K.D., Spalart, P.R.: An approach to wall modeling in large-eddy simulations. Phys. Fluids **12**, 1629–1632 (2000)
8. Batten, P., Goldberg, U., Chakravarthy, S.: LNS—an approach towards embedded LES, AIAA Paper 2002-0427 (2002)
9. Batten, P., Goldberg, U., Chakravarthy, S.: Interfacing statistical turbulence closures with large-eddy simulation. AIAA J. **42**, 485–492 (2004)
10. Davidson, L., Billson, M.: Hybrid LES/RANS using synthesized turbulence for forcing in the interface. Int. J. Heat Fluid Flow **28**, 1028–1042 (2006)
11. Jarrin, N., Benhamadouche, S., Laurence, D., Prosser, R.: A synthetic-eddy-method for generating inflow conditions for large-eddy simulation. Int. J. Heat Fluid Flow **27**, 585–593 (2006)
12. Mathey, F., Cokljat, D., Bertoglio, J.P., Sergent, E.: Specification of inlet boundary condition using vortex method. In: Hanjalic, K., Nagano, Y., Tummers, M. (eds.) Turbulence, Heat and Mass Transfer 4. Begell House Inc. (2003)
13. Lund, T.S., Wu, X., Squires, K.D.: Generation of turbulent inflow data for spatially-developing boundary layer simulations. J. Comput. Phys. **140**, 233–258 (1998)
14. Spalart, P.R., Strelets, M.Kh., Travin, A.K.: Direct numerical simulation of large-eddy-break-up devices in a boundary layer. Int. J. Heat Fluid Flow **27**, 902–910 (2006)
15. Spalart, P.R., Allmaras, S.R.: A one-equation turbulence model for aerodynamic flows. La Rech. Aerospatiale. **1**, 5–21 (1994)
16. Spalart, P.R., Deck, S., Shur, M.L., Squires, K.D., Strelets, M.Kh., Travin, A.K.: A new version of detached-Eddy simulation, resistant to ambiguous grid densities. Theor. Comput. Fluid Dyn. **20**, 181–195 (2006)
17. Shur, M.L., Spalart, P.R., Strelets, M.Kh., Travin, A.K.: Improvement of delayed detached-Eddy simulation for LES with wall modeling. Int. J. Heat Fluid Flow **29**, 1638–1649 (2006)
18. Gleyzes, C., Capbern, P.: Experimental study of two AIRBUS-ONERA airfoils in near stall conditions. Aerosp. Sci. Technol. **7**, 439–449 (2003)
19. LESFOIL: Large-Eddy Simulation of Flow around a High Lift Airfoil. Davidson, L., Cokljat, D., Fröhlich, J., Lesczíner, M.A., Mellen, C., Rodi, W. (eds.) Notes on Numerical Fluid Mechanics and Multidisciplinary Design. 83. Springer, Berlin (2003)
20. Nolin, G., Mary, I.: Test Case 06: A-airfoil. http://cfd.mace.manchester.ac.uk/desider/private/meeting-docs/file_meet-115287900506_ONERA.tar (2007). Accessed 28 August 2010
21. Strelets, M.: Detached Eddy Simulation of massively separated flows. AIAA Paper 2001-0879 (2001)
22. Rogers, S.E., Kwak, D.: An upwind differencing scheme for the time-accurate incompressible Navier-Stokes equations. AIAA Paper 1988-2583-CP (1988)
23. Roe, P.L.: Approximate Rieman solvers, parameter vectors and difference schemes. J. Comput. Phys. **46**, 357–378 (1981)